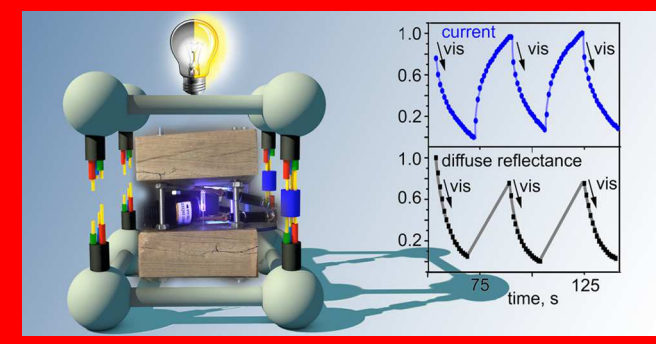


# Connecting Wires: Photoinduced Electronic Structure Modulation in Metal-Organic Frameworks

Ekaterina A. Dolgopolova, Vladimir A. Galitskiy, Corey R. Martin, Haley N. Gregory, Brandon J. Yarbrough, Allison M. Rice, Anna A. Berseneva, Otega A. Ejegbaywo, Kenneth S. Stephenson,<sup>‡</sup> Preecha Kittikhunnatham,<sup>†</sup> Stavros G. Karakalos,<sup>§</sup> Mark D. Smith,<sup>†</sup> Andrew B. Greytak, Sophya Garashchuk, and Natalia B. Shustova\*, o

Supporting Information

Electronic structure modulation of metalorganic frameworks (MOFs) through the connection of linker "wires" as a function of an external stimulus is reported for the first time. The established correlation between MOF electronic properties and photoisomerization kinetics as well as changes in an absorption profile is unprecedented for extended well-defined structures containing coordinatively integrated photoresponsive linkers. The presented studies were carried out on both single crystal and bulk powder with preservation of framework integrity. An LED-containing electric circuit, in which the switching behavior was driven by the changes in MOF electronic profile, was built for



visualization of experimental findings. The demonstrated concept could be used as a blueprint for development of stimuliresponsive materials with dynamically controlled electronic behavior.

## ■ INTRODUCTION

Modulation of electronic structure as a function of external stimuli is driven by multifunctional device development. 1-5 For instance, optical control over material electronic structures offers a powerful approach for optical switch integration, memory device evolution, and photocatalysis. <sup>6–13</sup> Tailoring electronic properties of metal-organic frameworks (MOFs) was previously achieved through metal node engineering, redox-active linker installation, or guest incorporation. 14-23

Herein, we demonstrate the first studies of electronic structure modulation of MOFs through connection of linker "wires" using two classes of photoresponsive ligands possessing distinct photoisomerization kinetics (Scheme 1). In particular, we show that tunability of electronic properties of crystalline three-dimensional (3D) frameworks with covalently integrated photochromic units results in changes in the diffuse reflection (DR) profile of the material that varies as a function of the excitation wavelength. Moreover, such cycling of electronic properties occurs with preservation of framework integrity. We present electronic structure modulation of MOF bulk and single crystal (including two new structures for which synthetic and characterization details are provided). The change in electronic structure also results in conductivity modulation, which could be visualized using an electronic circuit connected to a light-emitting diode (LED, Scheme 1).

# RESULTS AND DISCUSSION

To correlate changes between MOF electronic profile and photoisomerization kinetics of photochromic molecules, such molecules can be linked together via the frameworks to form an "electric circuit". 24,25 To build such a circuit, we integrated stimuli-responsive ligands as a part of the framework (Scheme 1). Two distinct classes of linkers with spiropyran and diarylethene cores have been chosen as examples with drastically different photoisomerization mechanisms. For instance, switching of spiropyran derivatives from a neutral spiropyran form to a charge-separated merocyanine zwitterion (Figure 1) induces a change in the conjugation pattern and charge distribution. Spiropyran isomerization also imposes a change in the molecular conformation, requiring significant structural freedom. In particular, the mechanism of spiropyran isomerization involves electron delocalization, caused by excitation, resulting in breaking the C-O bond as well as rearrangement and twist of two parts of the molecule leading to a planar isomer. Unlike spiropyran, diarylethene derivatives are capable of fast photoisomerization in the solid state since the covalent bond formation between the methylthiophene groups occurs within the plane (Figures 2

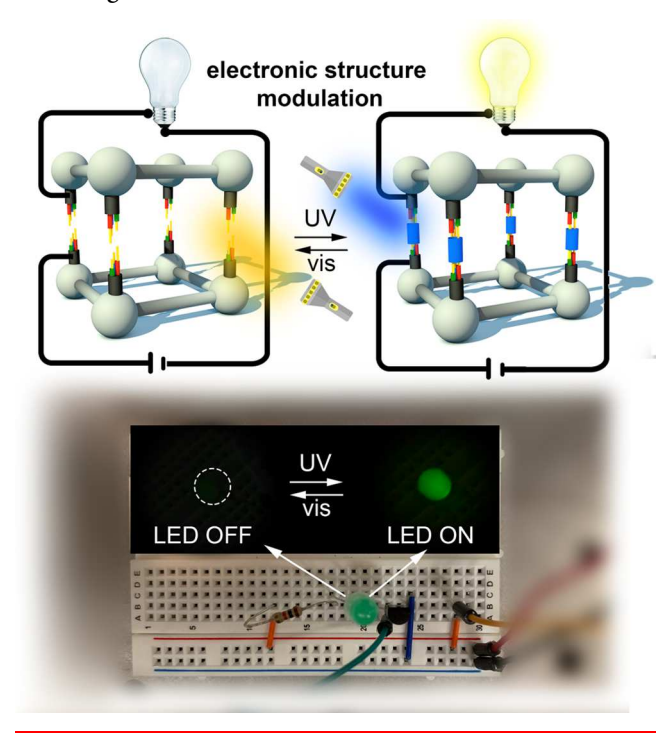
Received: December 28, 2018 Published: March 6, 2019

5350

<sup>&</sup>lt;sup>†</sup>Department of Chemistry and Biochemistry, University of South Carolina, Columbia, South Carolina 29208, United States \*Department of Physics and Astronomy, University of South Carolina, Columbia, South Carolina 29208, United States §College of Engineering and Computing, University of South Carolina, Columbia, South Carolina 29208, United States

Journal of the American Chemical Society

Scheme 1. (Top) "Wiring" Stimuli-Responsive Linkers as a Function of Excitation Wavelength for Framework Electronic Structure Modulation; (Bottom) Visualization of Changes of MOF Electronic Properties through LED Switching



and 4).27,32-38 The photoisomerization process (open to closed form, Figures 2 and 4) results in  $\pi$ -conjugation extension, which could lead to higher molecular conductance.27 The major challenge is translating changes at the molecular level to bulk properties of the material without framework decomposition.

Specifically, we studied the possible correlation between the photoisomerization process and the electronic properties as a function of an excitation wavelength on four frameworks with photochromic ligands (Figures 1, 3, and 4) and three "photoinactive" frameworks as control experiments. The initial studies were carried out on Zn<sub>2</sub>(DBTD)(TNDS) (1, H<sub>4</sub>DBTD = 3',6'-dibromo-4',5'-bis(4-carboxyphenyl)-1[1,1':2',1"-tetraphenyl]-4,4"-dicarboxylic acid, TNDS = 1',3',3'-trimethyl-6nitro-4',7'-di(pyridin-4-yl)spiro[chromene-2,2'-indoline], Figure 1),<sup>39</sup> in which spiropyran units were attached to the linker backbone and able to undergo photoisomerization inside the framework pores. The structure of 1 consists of tetracarboxylate linkers, DBTD<sup>4-</sup>, connected by zinc-paddle-wheel nodes and TNDS bound to axial positions of these nodes (Figure 1).

To estimate the effect of spiropyran photoisomerization on the MOF electronic structure, we examined the absorption properties of 1 upon alternation of excitation wavelengths (Figures 1 and S1-S4). After 365 nm irradiation, a bathochromic shift of the absorption profile was detected (Figure S2), resulting in changes of the optical band gap from 1.87 to 1.73 eV (Figure S3). Figure 1 demonstrates that the spiropyran and merocyanine forms of TNDS could interconvert upon irradiation without framework degradation, even after several consecutive irradiation cycles (see Supporting Information (SI), Figure S1). Thus, these studies demonstrate the possibility of optical cycling for a spiropyran

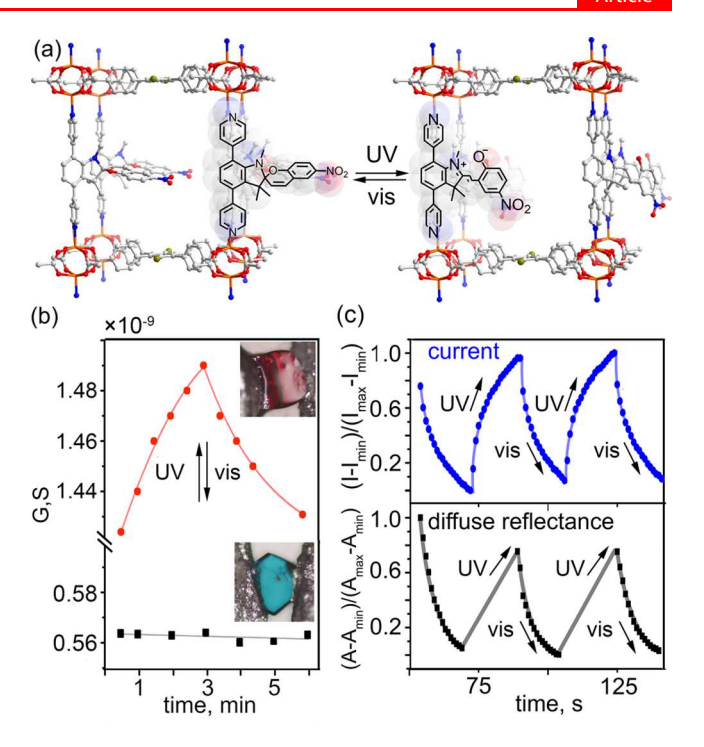


Figure 1. (a) Single-crystal X-ray structures of 1 with simulated spiropyran moieties demonstrating spiropyran-to-merocyanine photoisomerization. Orange, red, blue, brown, and gray spheres represent zinc, oxygen, nitrogen, bromine, and carbon atoms, respectively. (b) Changes in conductance of a single crystal of 1 (red) and Cu<sub>3</sub>(BTC)<sub>2</sub> (black, control experiment) upon 365 nm irradiation, followed by 590 nm irradiation. Insets show photographs of the single-crystal setups. (c) Normalized optical cycling of current (top) and absorption (bottom) as a function of alternating irradiation.

derivative integrated as a part of the extended crystalline structure.

For correlation of photoisomerization with changes in MOF conductivity, we used a home-built two-contact probe pressedpellet setup (2C3PS)<sup>20,41</sup> allowing for simultaneous MOF irradiation and monitoring of changes in electric current flow in a compressed powder sample under a constant applied voltage. We found that 365 nm irradiation for only 15 s led to approximately 1.2 times increase in the conductivity of 1. The absolute ratio between conductivity values corresponding to spiropyran and merocyanine forms was not feasible to measure due to fast cycloreversion kinetics (i.e., spontaneous transition of the merocyanine state back to the spiropyran form). However, we were able to study photoisomerization kinetics of the spiropyran moiety under ultraviolet (UV) irradiation (i.e., spiropyran-to-merocyanine photoconversion) and reverse cyclization under visible-light irradiation based on the rate of change of the electric response of 1. The forward rate  $(k_{UV})$ and reverse rate  $(k_{\rm vis})$  constants were found to be  $7.6 \times 10^{-2}$  $s^{-1}$  and  $2.2 \times 10^{-2} s^{-1}$ , respectively, considering a first-order response.<sup>39</sup>

After establishing the photophysics-resistivity correlation for the bulk powder of 1, two-probe conductivity measurements on a single crystal were carried out (Figure 1). To promote ring-opening photoisomerization, a single crystal of 1 was irradiated at 365 nm for 3 min, followed by 3 min irradiation with 590 nm to stimulate reverse conversion of merocyanine to spiropyran. In agreement with the powder measurements, electrical conductance for the single crystal of 1

Journal of the American Chemical Society

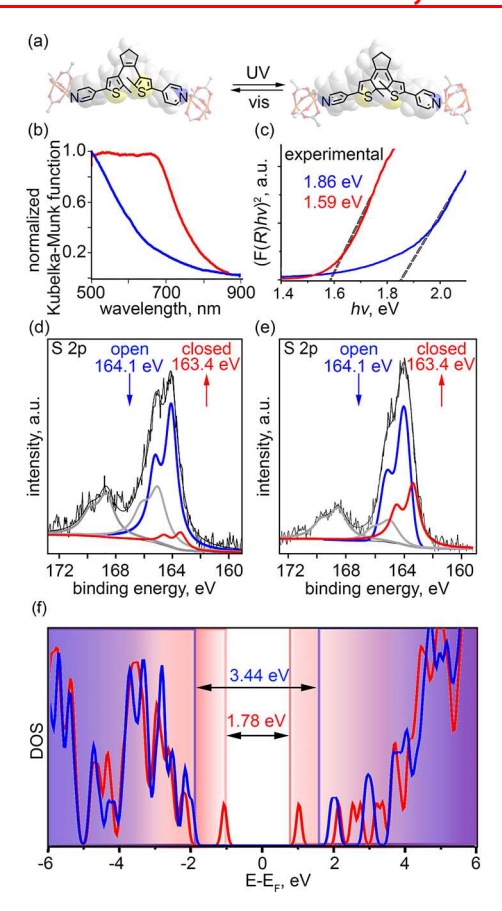


Figure 2. (a) Photoisomerization of BPMTC coordinated to Zn<sub>2</sub>(O<sub>2</sub>C-)<sub>4</sub> nodes. (b, c) Experimental DR spectra and Tauc plot  $([F(R) \times h\nu]^2 \text{ vs } h\nu)$  of 2 before (blue) and after (red) irradiation  $(\lambda_{ex} = 365 \text{ nm}, t = 10 \text{ min}). (d, e)$  XPS data of 2 for the S(2p) region before (d) and after (e) irradiation ( $\lambda_{ex} = 365$  nm, t = 30 min). (f) Simulated density of states of a truncated MOF model in the "open" (blue) and "closed" (red) forms.

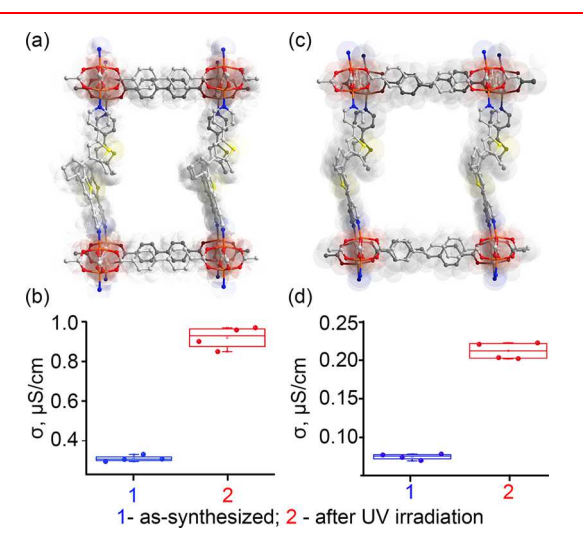


Figure 3. (Top) Single-crystal X-ray structures of (a) 2 and (c) 2'. Orange, red, blue, yellow, and gray spheres represent zinc, oxygen, nitrogen, sulfur, and carbon atoms, respectively. (Bottom) Conductivity data for (b) 2 and (d) 2' before (blue) and after (red) UV irradiation ( $\lambda_{\text{ex}} = 365 \text{ nm}, t = 2 \text{ h}$ ).

increased while the original value was restored after 590 nm irradiation.

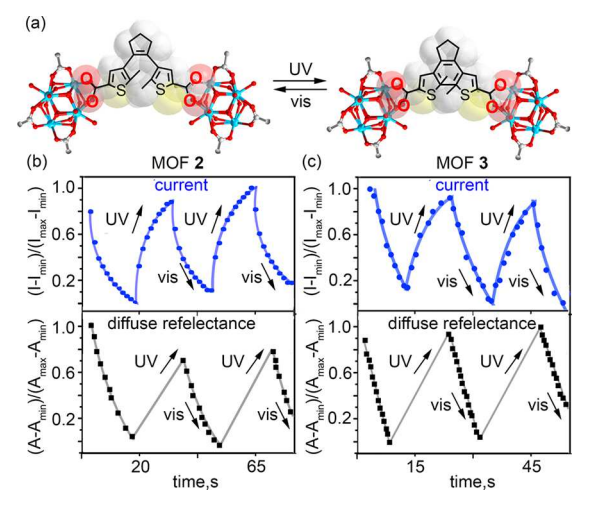


Figure 4. (a) Photoisomerization of BCMTC<sup>2-</sup> coordinated to  $Zr_6O_4(OH)_8^{8+}$  nodes. (b and c) Normalized optical cycling of current (top) and absorption (bottom) of 2 (b) and 3 (c) as a function of alternating irradiation ( $\lambda_{ex} = 365 \text{ nm (UV)}$ ).

As a control experiment, we performed the same cycling studies on both single-crystal and bulk forms for two MOFs without photochromic units, Zn<sub>2</sub>(DBTD)(DPB-CHO) (DPB-CHO = 2,5-di(pyridin-4-yl)benzaldehyde, Figures S5-S7)<sup>42</sup> and  $Cu_3(BTC)_2$  (H<sub>3</sub>BTC = benzene-1,3,5-tricarboxylic acid). 22,43 We synthesized novel Zn<sub>2</sub>(DBTD)(DPB-CHO) isostructural to 1; however, Zn<sub>2</sub>(DBTD)(DPB-CHO) does not contain photoactive spiropyran units. In addition, the Cu<sub>3</sub>(BTC)<sub>2</sub> framework was chosen due to its well-studied physicochemical properties. 19,22 As expected, modulation of the electric response was not detected for these frameworks in either single-crystal or bulk forms (Figures S4 and S7), confirming that only the photochromic units in 1 are responsible for observed electric response modulation.

To visualize the concept of electronic structure changes upon irradiation with light, we built a single-transistor amplifier circuit on a breadboard, allowing an LED to indicate the previously detected changes (Schemes 1 and S1). The 2C3PS containing 1 was incorporated as a resistor in series with the base in a common-emitter circuit, with the LED attached to the collector. As expected, upon irradiation of 1 with UV light, the LED was illuminated, while removal of UV irradiation and leaving the sample in the dark resulted in the LED being turning off.

Unlike spiropyran-based molecules, diarylethene derivatives do not undergo reverse photoisomerization spontaneously.<sup>2</sup> To establish the photophysics-electronic structure correlation for diarylethene linkers similarly to that of TNDS, we prepared three frameworks containing bis(5-pyridyl-2-methyl-3-thienyl)cyclopentane ligands (BPMTC, Figure 2) and 4,4'-(cyclopent-1-ene-1,2-diyl)bis(5-methylthiophene-2-carboxylic acid) (H<sub>2</sub>BCMTC, Figures 4 and S17), 44,45 in which the photochromic moiety was a part of the ligand backbone. Two of the prepared 3D frameworks, Zn<sub>2</sub>(BPDC)<sub>2</sub>(BPMTC) (2) and Zn<sub>2</sub>(SDC)<sub>2</sub>(BPMTC) (2'), consist of Zn-based paddle-wheel units connected by BPDC<sup>2-</sup> (2, H<sub>2</sub>BPDC = biphenyl-4,4'-dicarboxylic acid, Figures 3, S8, and S9)<sup>28</sup> or SDC<sup>2-</sup> (2', H<sub>2</sub>SDC = stilbene-4,4'-dicarboxylic acid, Figures 3 and S10-S14), while the photochromic BPMTC is axially coordinated to the nodes. Notably, in many cases, utilization of pyridylcontaining photochromic linkers with ditopic ligands (e.g.,

terephthalic acid) results in formation of exclusively interpenetrated frameworks, \$39,46-48\$ allowing release of strain energy by local and global structural changes in the framework itself. As a result of such framework behavior, the photoisomerization rate of BPMTC integrated into the interpenetrated framework structure was shown to mimic the behavior of the photoresponsive linker in solution. In 2 or 2′, the carbon atoms in the thienyl groups were found to be located in close proximity to each other (<4.2 Å), indicating the possibility for the photocyclization reaction.

The presence of sulfur in BPMTC provided for the unique opportunity to apply X-ray photoelectron spectroscopy (XPS) to study linker photoisomerization by monitoring changes in the S(2p) region due to different binding energies of the two isomers (Figure 2). "Open-to-closed" conversion was induced by exposure to UV irradiation during XPS data collection. The S(2p) region for "open" BPMTC is characterized by a doublet at 164.1 eV, while the S(2p) spectrum of the "closed" form is shifted toward a lower binding energy (163.4 eV). "Under UV irradiation, a growth in the peak intensity corresponding to the "closed" form and simultaneous decrease of the peak intensity corresponding to the "open" form were recorded. As a result, the amounts of the "closed" isomer increased by 28% and 12% after UV irradiation in 2 and 2', respectively (Figures 2, S9, and S14).

To correlate BPMTC photoisomerization with changes in electronic properties, DR spectroscopy and theoretical calculations were employed. Upon 365 nm irradiation for 10 min, a bathochromic shift of the absorption profile of 2 was observed (Figure 2). The estimated optical band gaps of 2 before and after irradiation were found to be 1.86 and 1.59 eV, respectively (Figure 2). A similar behavior was observed for 2' (Figures S12 and S13). To rationalize the observed changes, we carried out theoretical calculations on a truncated MOF model (Figure 2). Time-dependent density-functional-theory calculations revealed that BPMTC isomerization from the "open" to "closed" form results in a decrease of the framework band gap, which supports experimental observations (Figures 2, 3, S12, and S13). See Experimental Section for computational details and analysis.

To investigate the changes in electronic structure upon irradiation with UV light for BPMTC-containing MOFs, we utilized the 2C3PS described above. 20,41 The studies were performed on bulk of 2 and 2' because of their growth as crystalline conglomerates consisting of small, nonuniformly shaped single crystals. The electrical conductivity of the prepared pellets was calculated by fitting the obtained linear I-V curves using Ohm's law. A total number of six pressed pellets from separate batches of the material were used. The details regarding sample preparation and measurements can be found in the Experimental Section. Equal variance t-test analysis was used for the comparison of the measured conductivity values. So The obtained p-tail value was less than 0.05, indicating a statistical difference between values for as-synthesized and irradiated MOFs (Figure 3). Thus, average conductivity values for the non-irradiated sample were found to be  $(6.4 \pm 0.87) \times$  $10^{-7}$  (2) and  $(9.5 \pm 2.1) \times 10^{-7}$  S × cm<sup>-1</sup> (2'), while after UV irradiation, approximately 3-times conductivity enhancement was detected ((1.7  $\pm$  0.34)  $\times$  10<sup>-6</sup> S  $\times$  cm<sup>-1</sup> (2) and (2.9  $\pm$ 0.67) ×  $10^{-6}$  S × cm<sup>-1</sup> (2')). These measurements are the first examples of changes in electronic behavior of crystalline materials containing diarylethene compounds.

To further examine the influence of linker photoisomerization on electronic structure changes of 2, we performed a correlation of changes in absorption profile with changes in electric response upon alternation of excitation wavelength. As shown in Figure 4, the absorbance profile and electric response of 2 can be reversibly switched between two states for at least three consequent irradiation cycles (t = 5 s, Figure 4).

In the case of the  $\rm H_2BCMTC$  linker (Figures 4 and S17), the photochromic ligand was coordinatively installed in the prepared Zr-MOF through a postsynthetic modification procedure, resulting in the formation of 3 (Figures 4 and S18-S22). <sup>39</sup> For that, we utilized the  $\rm Zr_6O_4(OH)_8(Me_2BPDC)_4^{51}$  MOF ( $\rm Zr_6(Me_2BPDC)_4$ ,  $\rm H_2Me_2BPDC=2,2'$ -dimethylbiphenyl-4,4'-dicarboxylic acid), where coordination of an additional linker with carboxylate groups, BCMTC<sup>2-</sup>, occurs through replacement of OH<sup>-</sup> and  $\rm H_2O$  groups at the Zr-based metal node (Figures 4 and S18). Flexibility of the parent Zr-framework allows for accommodation of structural changes associated with BCMTC<sup>2-</sup> isomerization.

Similar to 1 and 2, we studied the changes in an absorption profile of 3 upon alternation of an excitation wavelength (Figure 4). We showed that the interconversion of the "open" form of the BCMTC<sup>2-</sup> linker in 3 to the "closed" isomer is possible for several cycles. Correlation of changes in the DR profile with those in the electronic structure was performed using the 2C3PS (Figure 4). The electrical conductivity of the prepared pellets was calculated based on the foregoing method. The average conductivity values for the pressed pellets increased 2 times after *in situ* irradiation inside the 2C3PS for 1 h  $((1.4 \pm 0.32) \times 10^{-5} \text{ S} \times \text{cm}^{-1}$  and  $(2.3 \pm 0.17) \times 10^{-5} \text{ S} \times \text{cm}^{-1}$  before and after irradiation, respectively).

As a control experiment, we performed a similar cycling experiment for its parent framework  ${\rm Zr_6(Me_2BPDC)_4}$  without photochromic moieties (see details in the Experimental Section, Figure S21). As expected, no changes in the electric response of  ${\rm Zr_6(Me_2BPDC)_4}$  were detected upon irradiation, while 3 showed a reversible modulation of the electric response (Figure S22). These measurements are in line with the possibility of electronic structure modulation as a function of external light as observed for the 2 and 2' frameworks.

## CONCLUSION

To summarize, the presented results are the first proof-ofprinciple demonstration of photoinduced electronic structure modulation of frameworks consisting of two distinct classes of photochromic molecules with drastically different photoisomerization kinetics. In the case of the spiropyran-based linker, formation of a charge-separated merocyanine form under UV irradiation increases delocalization of the frontier orbitals and decreases their spatial separation and, therefore, could result in an increase of charge-hopping rates, promoting conductivity enhancement.<sup>23</sup> The enhanced charge transport for diarylethene derivatives could be attributed to the changes in the  $\pi$ -conjugation length upon the photocyclization reaction.<sup>52</sup> For the example of photochromic compounds coordinatively integrated inside the scaffold, we performed a correlation of photophysics with changes in conductivity in extended crystalline materials for the first time, which could be interpreted based on electronic structure calculations. Moreover, the possibility of electric response cycling and its correlation with photoisomerization processes was demonstrated for spiropyran-containing crystalline materials for the

first time. Furthermore, electronic structure investigations were performed for both bulk and single-crystal forms supported by results from control experiments. By utilization of XPS, we showed that the photoisomerization process for diarylethene-based linkers integrated into a framework can be monitored *in situ*. Finally, to visualize MOF conductivity changes, we constructed an electric circuit allowing for performance of LED switching as a function of incident light. Thus, we provided a pathway for translation of changes occurring on a molecular level (linker) into properties of bulk materials, which could be used as a blueprint for the development of stimuliresponsive materials with dynamically controlled electronic properties.

## EXPERIMENTAL SECTION

Materials. Zinc nitrate, hexahydrate (lab grade, Ward's Science), copper(II) nitrate, hemi(pentahydrate) (98.3%, Mallinckrodt AR), tin(II) chloride, anhydrous (98%, Beantown Chemicals), copper(I) chloride, anhydrous (97%, Strem Chemicals), bis-(triphenylphosphine)palladium(II) dichloride (96%, Oakwood Chemical), copper powder (99.9%, Alfa Aesar), sodium carbonate (ACS grade, Ameresco), magnesium sulfate, anhydrous (USP, Chem-Implex, International Inc.), sodium sulfate, anhydrous (99.5%, Oakwood Chemical), sodium hydroxide (ACS, Oakwood Chemical), sodium nitrite (98%, Oakwood Chemical), chromium(VI) oxide (99.9%, Sigma-Aldrich), sodium carbonate (ACS grade, Macron Fine Chemicals), potassium carbonate (lab grade, Ward's Science), aluminum chloride, anhydrous (95+%, Alfa Aesar), tetrakis-(triphenylphosphine)palladium(0) (98%, Matrix Scientific), titanium chloride (99%, Beantown Chemicals), zinc dust (99.3%, Fisher Chemical), bromine (99.8%, Acros-Organic), 2,5-dibromonitrobenzene (99%, Oakwood Chemical), 3-methyl-2-butanone (98%, Beantown Chemicals), methyl trifluoromethanesulfonate (97%, Matrix Scientific), 2-hydroxy-5-nitrobenzaldehyde (98%, Oakwood Chemical), pyridine-4-boronic acid (95%, Matrix Scientific), 1,3,5benzenetricarboxylic acid (98%, Alfa Aesar), hexabromobenzene (>99%, TCI America), p-tolylmagnesium bromide (0.5 M in diethyl ether, Acros Organics), 4,4'-biphenyldicarboxylic acid (97%, Oakwood Chemical), stilbene-4,4'-dicarboxylic acid (98%, AK Scientific), 2,5-dibromotoluene (98%, Oakwood Chemical), 2-methylthiophene (98%, Matrix Scientific), N-chlorosuccinimide (98%, Sigma-Aldrich), glutaryl chloride (Oakwood Chemical), 4-bromopyridine hydrochloride (98%, Matrix Scientific), tri-n-butyl borate (98%, Strem Chemicals), n-butyllithium solution (1.6 M in hexanes, Sigma-Aldrich), hydrochloric acid (34.5-38%, ACS, VWR Chemicals), glacial acetic acid (ACS grade, BDH), sulfuric acid (ACS plus grade, Fisher Chemical), nitric acid (ACS reagent, Sigma-Aldrich), fluoroboric acid (48%, Oakwood Chemical), acetic anhydride (99.63%, Chem-Impex International Inc.), benzene (ACS grade, Beantown Chemicals), carbon disulfide (99.9%, HoneyWell), ethylene glycol (semi grade, VWR Analytics), carbamide (98+%, Alfa Aesar), toluene (ACS grade, Macron Fine Chemicals), dichloromethane (ACS grade, Oakwood Chemical), ethyl acetate (HPLC grade, EMD Chemicals), ethanol (200 proof, Decon Laboratories, Inc.), methanol (HPLC plus grade, Sigma-Aldrich), acetone (ACS grade, Sigma-Aldrich), chloroform (99.9%, Fisher Chemical), ethyl ether anhydrous (ACS grade, Fisher Chemical), hexanes (ACS, BDH), N,N-dimethylformamide (>99%, Tokyo Chemical Industry), piperidine (99%, Sigma-Aldrich), carbon tetrachloride (99.9%, Sigma-Aldrich), tetrahydrofuran (HPLC grade, Beantown Chemicals), chloroform-d (99.8%, Cambridge Isotopes), acetone-d<sub>6</sub> (99.9%, Cambridge Isotopes), and dimethyl sulfoxide-d<sub>6</sub> (99.9%, Cambridge Isotopes) were used as received.

The compounds 1, <sup>3</sup> 9 2, <sup>3</sup> 9 3, <sup>3</sup> 9 Cu<sub>3</sub>(BTC)<sub>2</sub>, <sup>43</sup>, Zr<sub>6</sub>(Me<sub>2</sub>BPDC)<sub>4</sub>, <sup>51</sup>H<sub>4</sub>DBTD, <sup>53</sup> DPB-CHO, <sup>42</sup> and BPMTC<sup>44</sup> were prepared according to reported literature procedures.

Preparation of Zn<sub>2</sub>(DBTD)(DPB-CHO). The Zn<sub>2</sub>(DBTD)(DPB-CHO) MOF was prepared using a slightly modified literature

procedure.<sup>53</sup> In a one-dram vial, Zn(NO<sub>3</sub>)<sub>2</sub>·6H<sub>2</sub>O (18.0 mg, 60.5  $\mu$ mol), H<sub>4</sub>DBTD (5.40 mg, 7.50  $\mu$ mol), and DPB-CHO (5.00 mg, 19.2  $\mu$ mol) were dissolved in a mixture of 0.8 mL of N,Ndimethylformamide (DMF) and HBF<sub>4</sub> (6 µL) followed by sonication. The resulting solution was placed in a preheated oven at 80 °C for 24 h and then cooled to room temperature over 2 h. Colorless crystals of  $Zn_2(DBTD)(DPB-CHO)$  (4.70 mg, 4.27  $\mu$ mol) were isolated in 57% yield. A detailed description of the crystallographic data collection and refinement details is given in Table S1. The determined structure of  $Zn_2(DBTD)(DPB-CHO)$  is shown in Figure S5. FTIR (neat, cm<sup>-1</sup>): 2928, 1665, 1641, 1613, 1559, 1501, 1435, 1385, 1255, 1222, 1179, 1090, 1063, 1026, 1018, 905, 865, 845, 825, 787, 749, 725, and 658. The powder X-ray diffraction (PXRD) pattern of Zn<sub>2</sub>(DBTD)(DPB-CHO) matches the one simulated from single-crystal X-ray data (Figure S6). PXRD studies were also used to confirm crystallinity of the bulk material before and after irradiation (Figure S6). The PXRD patterns and modulation of electronic properties of Zn<sub>2</sub>(DBTD)-(DPB-CHO) as a function of the excitation wavelength in the bulk and single-crystal forms are shown in Figures S6, S7, and S4.

Preparation of 2'. In a 20 mL vial, Zn(NO<sub>3</sub>), 6H<sub>2</sub>O (7.00 mg, 23.5 µmol), 4,4'-stilbenedicarboxylic acid (H<sub>2</sub>SDC, 6.50 mg, 24.2  $\mu$ mol), and BPMTC (10.0 mg, 41.3  $\mu$ mol) were dissolved in 5 mL of DMF followed by sonication. The resulting solution was heated at 110  $^{\circ}\text{C}$  in an isothermal oven. After 24 h, the reaction mixture was cooled to room temperature over 2 h. Brown wedge-shaped crystals of 2' (15.8 mg, 17.5  $\mu$ mol) were isolated in 75% yield. A detailed description of the crystallographic data collection and refinement details is given in Table S1. The determined structure of 2' is shown in Figures 3 and S10. FTIR (neat, cm<sup>-1</sup>): 3469, 2932, 1659, 1639, 1606, 1541, 1506, 1387, 1255, 1223, 1180, 1091, 1031, 1015, 979, 961, 866, 855, 825, 804, 786, 708, 684, and 659. As shown in Figure S11, the PXRD pattern of 2' matches the one simulated from singlecrystal X-ray data. Moreover, PXRD studies were used to confirm the crystallinity of the bulk material before and after irradiation with UV light (Figure S11). The PXRD patterns, diffuse reflectance spectra for "open" and "closed" form of the linker, Tauc plots, XPS, and conductivity data are shown in Figures S11-S14 and 3, respectively.

Electronic Structure as a Function of External Stimuli. To study the possibility of MOF electronic structure modulation as a function of an excitation wavelength, we used a 2C3PS similar to previously reported examples.<sup>20,41</sup> An "in-house" apparatus made it possible to fabricate the pressed pellets and perform measurements in situ. The MOF crystalline powder (10 mg), predried for 1 h in air, was pressed between two stainless steel rods inside an insulating quartz tube. The diameter of the resulting pellet is the same as the inner diameter of the quartz tube (d = 2 mm). The thickness of the pellets was kept consistent (l = 1 mm) by using the same amount of material. After forming a small pellet, the stainless-steel rods were connected to a sourcemeter (Keithley Instruments GmbH, Germering, Germany, model 263 or 2636A) and an electrometer (Keithley Instruments GmbH, Germering, Germany, model 617) using alligator clips to perform conductivity measurements. The measurements were performed under the same conditions (at room temperature in the dark), unless otherwise noted.

Dependence of the current values on an excitation wavelength for 1, 2, 2′, 3,  $\rm Zn_2(DBTD)(DPB\text{-}CHO)$ , and  $\rm Cu_3(BTC)_2$  was measured in the previously discussed 2C3PS, which was connected to a sourcemeter (Keithley Instruments GmbH, Germering, Germany, model 2636A, Figures 1 and S7). Constant voltage (5 V) was applied, while current was measured every 300 ms (number of power line cycles (NPLC) 5, delay of 1 ms). Before data collection, an equilibration time (t=90 s) was applied in the dark. Then, the sample was irradiated (t=5 s) using a high-powered LED (M365L2, Thorlabs,  $\lambda_{\rm ex}=365$  nm, the LED—sample distance = 2 cm, LEDD1B power supply set at 700 mA), followed by thermal relaxation in the dark (t=5 s). The procedure was repeated for eight consecutive irradiation cycles (Figures S4 and S22). PXRD studies were used to confirm the integrity of the MOFs after optical cycling (Figures S1, S6, S8, and S11).

To measure the electrical conductivity for 2 and 2' before and after irradiation with UV light, each batch was divided into two portions. The first portion of the sample was used for electrical measurements as is, while the second portion was irradiated with a mounted highpowered LED (M365L2, Thorlabs,  $\lambda_{ex}$  = 365 nm, distance = 6 cm, t = 2 h, LEDD1B power supply set at 700 mA). Due to the possibility of MOF degradation in air for an extended period of time, the crystals were covered with a thin layer of DMF. For MOF 3, the irradiation with UV light was performed in situ using the 2C3PS for 1 h. The measurements were performed using the 2C3PS connected to a sourcemeter (Keithley Instruments GmbH, Germering, Germany, model 263) and an electrometer (Keithley Instruments GmbH, Germering, Germany, model 617). The I-V curve was collected by supplying a voltage in the range from -19 V to +19 V. The electrical conductance in the prepared materials follows Ohm's law and was estimated by fitting the obtained linear I-V curves. PXRD studies were used to confirm the integrity of 2, 2', and 3 after conductivity measurements (Figures S8, S11, and S19).

Studies of modulation of the electronic structure using single crystals of 1, Zn<sub>2</sub>(DBTD)(DPB-CHO), and Cu<sub>3</sub>(BTC)<sub>2</sub> were performed by applying the previously reported literature procedures using a two-probe method.<sup>20,54</sup> For each measurement, single crystals of the MOF were placed on a dry glass slide and excess DMF was removed using filter paper. After that, the crystals were placed under Paratone-N oil to prevent the possibility of their decomposition. A uniform single crystal without visible cracks was selected under an optical microscope and transported using a needle to a new dry glass slide. The crystal was carefully integrated between two blocks of silver paste (PELCO) to form the desired ohmic contact (Figures 1 and S7). The prepared setup was placed onto a station equipped with tungsten probes controlled by two micromanipulators (Signatone S-725-PRM). Electrical contact was made by placing the probes into the silver paste close to the immobilized single crystal. The data points of I-V curves were collected every 30 s under irradiation with UV light (Lixada, 7W 25 LED,  $\lambda_{ex}$  = 365 nm, distance = 5 cm, t = 3 min) followed by irradiation with a high-powered LED (M590L3, Thorlabs,  $\lambda_{ex}$  = 590 nm, distance = 5 cm, LEDD1B power supply set at 500 mA). The changes in the electric response of single crystals, caused by alternating of light irradiation, was obtained by fitting I-Vcurves and plotting the estimated conductance values over time. For 1 and Zn<sub>2</sub>(DBTD)(DPB-CHO), the I-V curve was collected by supplying voltage in the range from -5 to 5 V with a step size of 1 V, scan rate of 5 NPLC, and delay of 1 ms using a sourcemeter (Keithley Instruments GmbH, Germering, Germany, model 2636A). For  $Cu_3(BTC)_2$ , an I-V curve was collected by supplying voltage in the range from -0.5 to 0.5 V with a step size of 0.1 V, scan rate of 5 NPLC, and a delay of 1 ms using a sourcemeter (Keithley Instruments GmbH, Germering, Germany, model 2636A).

Optical Cycling. Diffuse reflectance measurements were carried out using an Ocean Optics JAZ spectrometer. An Ocean Optics ICP-REF integrating sphere was connected to the spectrometer using a 450  $\mu$ m SMA fiber optic cable. Prior to time-resolved DR measurements, the sample background was subtracted to cut off the region, which does not correspond to photophysical behavior of the photochromic moieties integrated into the framework. A sample was placed between two microscope slides and attached to the top of the integrating sphere with electrical tape to prevent sample displacement. A mounted high-powered LED (M365L2, Thorlabs,  $\lambda_{ex}$  = 365 nm, distance = 1 cm, LEDD1B power supply set at 700 mA) was used for in situ irradiation of the sample for 15 s; then the sample was allowed to undergo photoinduced reversion on the top of the integration sphere for 15 s while a spectrum was collected every 500 ms. This procedure was repeated for five consecutive irradiation cycles (Figures and 4).

LED Amplifier Circuit. To visualize the concept of electronic structure changes upon irradiation with light, we built a circuit on a breadboard using the 2C3PS, a transistor (UTC, 2N3904-RA9), and an LED (Jameco Electronics, LTL-307EE) (Schemes 1 and S1). We utilized this circuit to visualize the correlation of the photoisomerization kinetics with changes of the MOF electronic structure.

The assembled circuit was used for control and switching of the LED as a function of the excitation wavelength. In Scheme S1, the 2C3PS, containing a pressed pellet of the MOF, was used as a resistor (R<sub>2</sub>) in the circuit. Upon reducing the resistance of the sample in the 2C3PS by UV irradiation, the current at the base of the transistor increases. As the base current rises above a certain value, the LED emission becomes visible. A green LED and current limiting series resistor R<sub>1</sub>, used to prevent the LED from burning out, were connected to the same source of voltage and to the collector of the transistor. The emitter of the transistor was connected to a ground. Voltage on the source meter (Keithley Instruments GmbH, Germering, Germany, model 2636A) was chosen to obtain a current value slightly less than what is required to turn the LED on (5 and 1.85 V for 1 and Zn<sub>2</sub>(DBTD)(DPB-CHO), respectively). The pressed pellet of the MOF was irradiated with a mounted high-powered LED (M365L2, Thorlabs,  $\lambda_{ex}$  = 365 nm, distance = 6 cm, LEDD1B power supply set at 700 mA) for 90 s and then turned off. In the case of 1, irradiation with UV light increased the current on the base of the transistor, allowing the LED to light up. During the control experiment with Zn<sub>2</sub>(DBTD)(DPB-CHO), no effect on the LED intensity was observed.

XPS Studies. The XPS studies on MOF samples were carried out using a Kratos AXIS Ultra DLD system equipped with a monochromatic Al Klpha source, a hemispherical analyzer, charge neutralizer, and a load lock chamber for rapid introduction of samples without breaking vacuum. The base pressure in the XPS analysis chamber was  $2 \times 10^{-9}$  Torr before sample introduction and  $\leq 2 \times 10^{-9}$ 10<sup>-8</sup> Torr during experiments. XPS data were collected with a step size of 0.06 eV and dwell times of 1 s for O(1s), C(1s), N(1s), S(2p), and Zn(2p) regions. A charge neutralizer was used to compensate for sample charging by bombarding the sample with low-energy electrons; electrons are generated by a hot filament, and the trajectories of the electrons toward the sample are controlled by electric and magnetic fields. Survey scans were acquired to establish that there were no contaminants introduced during the sample preparation. They were collected with a step size of 0.8 eV and dwell times of 0.3 s, and the following regions were collected for each sample unless otherwise specified: C(1s), O(1s), Zn(2p), S(2p), and

Regarding the assignment of sulfur oxidation states in both 2 and 2', the S(2p) peaks around 164.1 and 163.4 eV are attributed to "open" and "closed" forms of the BPMTC linker, respectively (Figures 2, S9, and S14). These binding energies are consistent with those that have been reported in the literature for the BPMTC linker itself.<sup>49</sup> The difference in peak positions can be explained by changes in extended conjugation through the whole molecule during the photoisomerization process.4

Other Physical Measurements. PXRD patterns were recorded on a Rigaku Miniflex II diffractometer with accelerating voltage and current of 30 kV and 15 mA, respectively. FTIR spectra were obtained on a PerkinElmer Spectrum 100. DR spectra were collected on an Ocean Optics JAZ spectrometer. An Ocean Optics ISP-REF integrating sphere was connected to the spectrometer using a 450  $\mu$ m SMA fiber optic cable. Samples were loaded in an 8.0 mm quartz sample cell, which was referenced to an Ocean Optics WS-1 Spectralon standard. A mounted high-powered LED (M365L2, Thorlabs,  $\lambda_{ex}$  = 365 nm, distance = 1 cm, LEDD1B power supply set at 700 mA) was used for in situ irradiation of the samples.

Computational Details. The photoisomerization mechanism of the diarylethene molecule has been studied theoretically by several research groups, using cluster electronic structure codes and ab initio nonadiabatic molecular dynamics. 55-57 The collective findings can be summarized as follows: in the ground electronic state,  $S_0$ , the "open" and "closed" ring isomers are separated by a high barrier of approximately 1.8 eV and are, therefore, thermally stable. The isomerization proceeds through the first excited electronic state,  $S_1$ , exhibiting a conical intersection (CI) with the ground potential energy surface (PES). The cyclization begins with the UV excitation of the "open"-form molecule to  $S_1$ , where it accesses the CI without a barrier. The molecule relaxes to either "open" or "closed" form on the

ground PES via the CI. In the reverse reaction, the vertical excitation to S1 corresponds to the visible light, and there is a barrier to the CI of about 0.6 eV.57

In relation to the current experiments, we have examined the electronic structure of the BPMTC linker connecting two Zncontaining metal nodes. The linker was considered in the "open" and "closed" forms of the central ring, reversibly switchable by the electromagnetic field in the UV-visible region of 350-750 nm or 1.65-4.1 eV. The results reported here were performed using the density functional B3LYP with Grimme's dispersion correction<sup>51</sup> employing the 6-31+G\*\* basis, unless otherwise noted. The electronic excitations are computed employing the time-dependent density functional theory (TDDFT) with and without the Tamm-Dancoff approximation (TDA). The calculations have been performed using Q-Chem 5.1 software.<sup>59</sup>

The molecular models are truncated structures of MOFs constructed from the experimental geometries. We have considered several models: (a) a single diarylethene linker coordinated to two metal nodes, (b) two diarylethene linkers with the metal node in the center, and (c) two diarylethene linkers coordinated to three metal nodes with additional BPDC<sup>2-</sup> linkers, using a smaller 6-31G basis. For comparison we have also considered an isolated the diarylethene molecule. For the molecular model (a), shown in Figure 2, the electrostatic charges on the metal nodes are about -0.4 and 0.2 for the "closed" and "open" isomers, respectively. The charges of the terminating pyridyl groups are 0.20 unit. The charge of each Zn atom is about 1.25 units of elementary charge.

We have tested several density functionals (B3LYP, TPPS, PBE, M06-2X) with the D3 dispersion correction.<sup>58</sup> The B3LYP functional gave the best agreement with the UV-vis spectra of the isolated ligand in the "open" and "closed" forms. All functionals yielded a strong excitation of ~1.8 eV (690 nm) for the "closed" switch, while for the "open" switch the optical gaps were (depending on the functional) 2.8-3.6 eV or in the range of 350-450 nm (Table S2). These values are consistent with previous studies of a similar photoswitch as the central part of linkers connected to the gold leads, whose HOMO-LUMO gaps were calculated as 1.73/3.58,60 1.7/ 3.1,61 and 2.34/3.6262 eV for the "closed"/"open" forms, respectively. The values were measured for the diarylethene thin films (1.2/3.4) and 1.5/3.1 eV)<sup>63</sup> and blends with P3HT and N2200 (2.24/3.86 and 2.26/3.86 eV).64 Thus, despite the limitation of our 119-atom truncated molecular model, we expect that the electronic structure of the "closed"/"open" BPMTC photoswitch is reasonably described by the selected theoretical method.

The UV-vis spectra obtained with the convolution of 0.2 eV and normalized to one over the range 200-1000 nm are given for the fully "closed" and "open" switch and also for the statistical mixture of 11% and 39% in the "closed" state describing the experimental conditions. Figures 2, S15, and S16 show the HOMO-LUMO energy levels and the optical gaps for the "closed" and "open" switch, aligned to the zero of total electronic energy (the vacuum level for a molecule).

The computed UV-vis spectrum for the "open" photoswitch differs from the experimental result consistent with smaller excitation energies. One reason for this discrepancy is the limitation of our truncated molecular model: most likely the delocalized character of the electronic orbitals due to the metal nodes is not captured. The periodic calculations, though known to underestimate the band gaps, are desirable to investigate this point.

Within the cluster code calculations, we have estimated the effect of the linker coupling through the metal nodes on the HOMO-LUMO gap and on the excitation energy within the TDDFT/TDA and TDDFT for an isolated linker and for the two linkers coordinated to the node. The results are given in Table S3. Coordination to the node has reduced the HOMO-LUMO gap by 0.28 eV (7.3%) for the "open" switch and by 0.05 eV (2.4%) for the "closed" switch. Within a simple model—the energy level splitting due to the coupling of two identical systems—these values give the estimates of coupling between the linker energy levels due to the nodes. The respective changes of the TDDFT lowest excitations show the same trend, a

reduction by 7.0% and 2.8% for the "open" and "closed" isomers. This provides some support for the idea that extension of the molecular model to more nodes and linkers will reduce the band gaps for both isomers, and the effect will be noticeably larger for the "open" switch.

Upon examination of the frontier molecular orbitals, shown in Figures S22 and S23, the HOMO-LUMO orbitals (or nearly degenerate pairs of orbitals) are largely localized on the diarylethene linkers. However, if a metal node is included between the two linkers (Figure S23), then, for the "open" isomer, we find the third orbital close in energy to the HOMO and localized on the node. The three HOMO orbitals (being within 0.2 eV) may describe a delocalized electronic state for the "open" linker. This is consistent with the argument that the metal node couples the linkers, resulting in the lowering of the vertical energy gap in the extended MOF structure compared to an isolated linker.

## ASSOCIATED CONTENT

# Supporting Information

The Supporting Information is available free of charge on the ACS Publications website at DOI: 10.1021/jacs.8b13853.

Additional experimental details, X-ray structure refinement data of prepared MOFs, PXRD, XPS, DR, conductivity measurements data, and computational details (PDF)

Crystallographic information for 2' (Zn<sub>2</sub>(SDC)<sub>2</sub>(BPMTC)), CCDC 1882569 (CIF)

Crystallographic information for Zn<sub>2</sub>(DBTD)(DPB-CHO), CCDC 1882570 (CIF) (CIF)

Crystallographic information for H<sub>2</sub>BCMTC, CCDC 1898510 (CIF)

# AUTHOR INFORMATION

# **Corresponding Author**

\*shustova@sc.edu

ORCID ®

Stavros G. Karakalos: 0000-0002-3428-5433 Natalia B. Shustova: 0000-0003-3952-1949

Notes

The authors declare no competing financial interest.

# ACKNOWLEDGMENTS

N.B.S. gratefully acknowledges support from the NSF CAREER Award (DMR-1553634), the Sloan Research Fellowship provided by the Alfred P. Sloan Foundation, and a Cottrell Scholar Award from the Research Corporation for Science Advancement. S.G. thanks the National Science Foundation and SC EPSCoR/IDeA Program under Grant Nos. CHE-1056188 and OIA-1655740/13020-GA27.

## REFERENCES

- (1) Kim, H.; Yang, S.; Rao, S. R.; Narayanan, S.; Kapustin, E. A.; Furukawa, H.; Umans, A. S.; Yaghi, O. M.; Wang, E. N. Water Harvesting from Air with Metal-Organic Frameworks Powered by Natural Sunlight. Science 2017, 356, 430-434.
- (2) Kalmutzki, M. J.; Hanikel, N.; Yaghi, O. M. Secondary Building Units as The Turning Point in the Development of the Reticular Chemistry of MOFs. Sci. Adv. 2018, 4, No. eaat9180.
- (3) Cohen, S. M. The Postsynthetic Renaissance in Porous Solids. J. Am. Chem. Soc. 2017, 139, 2855-2863.
- (4) Kung, C.-W.; Platero-Prats, A. E.; Drout, R. J.; Kang, J.; Wang, T. C.; Audu, C. O.; Hersam, M. C.; Chapman, K. W.; Farha, O. K.; Hupp, J. T. Inorganic "Conductive Glass" Approach to Rendering Mesoporous Metal-Organic Frameworks Electronically Conductive

- and Chemically Responsive. ACS Appl. Mater. Interfaces 2018, 10, 30532–30540.
- (5) Lustig, W. P.; Li, J. Luminescent Metal-Organic Frameworks and Coordination Polymers as Alternative Phosphors for Energy Efficient Lighting Devices. *Coord. Chem. Rev.* **2018**, 373, 116–147.
- (6) Logan, M. W.; Lau, Y. A.; Zheng, Y.; Hall, E. A.; Hettinger, M. A.; Marks, R. P.; Hosler, M. L.; Rossi, F. M.; Yuan, Y.; Uribe-Romo, F. J. Heterogeneous Photoredox Synthesis of *N*-hydroxyoxazolidinones Catalysed by Metal-Organic Frameworks. *Catal. Sci. Technol.* **2016**, *6*, 5647–5655.
- (7) Vogelsberg, C. S.; Uribe-Romo, F. J.; Lipton, A. S.; Yang, S.; Houk, K. N.; Brown, S.; Garcia-Garibay, M. A. Ultrafast Rotation in an Amphidynamic Crystalline Metal-Organic Framework. *Proc. Natl. Acad. Sci. U. S. A.* **2017**, *114*, 13613–13618.
- (8) Foster, M. E.; Sohlberg, K.; Allendorf, M. D.; Talin, A. A. Unraveling the Semiconducting/Metallic Discrepancy in Ni<sub>3</sub>(HITP)<sub>2</sub>. *J. Phys. Chem. Lett.* **2018**, *9*, 481–486.
- (9) Woellner, M.; Hausdorf, S.; Klein, N.; Mueller, P.; Smith, M. W.; Kaskel, S. Adsorption and Detection of Hazardous Trace Gases by Metal-Organic Frameworks. *Adv. Mater.* **2018**, *30*, 1704679.
- (10) Stassen, I.; Burtch, N.; Talin, A.; Falcaro, P.; Allendorf, M.; Ameloot, R. An Updated Roadmap for the Integration of Metal-Organic Frameworks with Electronic Devices and Chemical Sensors. *Chem. Soc. Rev.* **2017**, *46*, 3185–3241.
- (11) Zhai, Q.-G.; Bu, X.; Mao, C.; Zhao, X.; Feng, P. Systematic and Dramatic Tuning on Gas Sorption Performance in Heterometallic Metal-Organic Frameworks. *J. Am. Chem. Soc.* **2016**, *138*, 2524–2527.
- (12) Müller, K.; Helfferich, J.; Zhao, F.; Verma, R.; Kanj, A. B.; Meded, V.; Bléger, D.; Wenzel, W.; Heinke, L. Switching the Proton Conduction in Nanoporous Crystalline Materials by Light. *Adv. Mater.* **2018**, *30*, 1706551.
- (13) Kirchon, A.; Feng, L.; Drake, H. F.; Joseph, E. A.; Zhou, H.-C. From Fundamentals to Applications: A Toolbox for Robust and Multifunctional MOF Materials. *Chem. Soc. Rev.* **2018**, *47*, 8611–8638
- (14) Johnson, B. A.; Bhunia, A.; Fei, H.; Cohen, S. M.; Ott, S. Development of a UiO-Type Thin Film Electrocatalysis Platform with Redox-Active Linkers. *J. Am. Chem. Soc.* **2018**, *140*, 2985–2994.
- (15) Mulzer, C. R.; Shen, L.; Bisbey, R. P.; McKone, J. R.; Zhang, N.; Abruña, H. D.; Dichtel, W. R. Superior Charge Storage and Power Density of a Conducting Polymer-Modified Covalent Organic Framework. *ACS Cent. Sci.* **2016**, *2*, 667–673.
- (16) Xie, L. S.; Sun, L.; Wan, R.; Park, S. S.; DeGayner, J. A.; Hendon, C. H.; Dincă, M. Tunable Mixed-Valence Doping toward Record Electrical Conductivity in a Three-Dimensional Metal-Organic Framework. *J. Am. Chem. Soc.* **2018**, *140*, 7411–7414.
- (17) McGuirk, C. M.; Runčevski, T.; Oktawiec, J.; Turkiewicz, A.; Taylor, M. K.; Long, J. R. Influence of Metal Substitution on the Pressure-Induced Phase Change in Flexible Zeolitic Imidazolate Frameworks. J. Am. Chem. Soc. 2018, 140, 15924–15933.
- (18) Guo, Z.; Panda, D. K.; Maity, K.; Lindsey, D.; Parker, T. G.; Albrecht-Schmitt, T. E.; Barreda-Esparza, J. L.; Xiong, P.; Zhou, W.; Saha, S. Modulating the Electrical Conductivity of Metal-Organic Framework Films with Intercalated Guest  $\pi$ -Systems. *J. Mater. Chem.* C **2016**, *4*, 894–899.
- (19) Talin, A. A.; Centrone, A.; Ford, A. C.; Foster, M. E.; Stavila, V.; Haney, P.; Kinney, R. A.; Szalai, V.; El Gabaly, F.; Yoon, H. P.; Léonard, F.; Allendorf, M. D. Tunable Electrical Conductivity in Metal-Organic Framework Thin-Film Devices. *Science* **2014**, *343*, 66–69.
- (20) Sun, L.; Park, S. S.; Sheberla, D.; Dincă, M. Measuring and Reporting Electrical Conductivity in Metal-Organic Frameworks: Cd<sub>2</sub>(TTFTB) as a Case Study. *J. Am. Chem. Soc.* **2016**, *138*, 14772–14782.
- (21) Rice, A. M.; Dolgopolova, E. A.; Yarbrough, B. J.; Leith, G. A.; Martin, C. R.; Stephenson, K. S.; Heugh, R. A.; Brandt, A. J.; Chen, D. A.; Karakalos, S. G.; Smith, M. D.; Hatzell, K. B.; Pellechia, P. J.; Garashchuk, S.; Shustova, N. B. Stack the Bowls: Tailoring the

- Electronic Structure of Corannulene-Integrated Crystalline Materials. *Angew. Chem., Int. Ed.* **2018**, *57*, 11310–11315.
- (22) Dolgopolova, E. A.; Brandt, A. J.; Ejegbavwo, O. A.; Duke, A. S.; Maddumapatabandi, T. D.; Galhenage, R. P.; Larson, B. W.; Reid, O. G.; Ammal, S. C.; Heyden, A.; Chandrashekhar, M.; Stavila, V.; Chen, D. A.; Shustova, N. B. Electronic Properties of Bimetallic Metal-Organic Frameworks (MOFs): Tailoring the Density of Electronic States through MOF Modularity. *J. Am. Chem. Soc.* 2017, 139, 5201–5209.
- (23) Garg, S.; Schwartz, H.; Kozlowska, M.; Kanj, A. B.; Müller, K.; Wenzel, W.; Ruschewitz, U.; Heinke, L. Conductance Photoswitching of Metal-Organic Frameworks with Embedded Spiropyran. *Angew. Chem., Int. Ed.* **2019**, *58*, 1193–1197.
- (24) Kudernac, T.; Katsonis, N.; Browne, W. R.; Feringa, B. L. Nano-electronic Switches: Light-induced Switching of the Conductance of Molecular Systems. *J. Mater. Chem.* **2009**, *19*, 7168–7177.
- (25) Barachevsky, V. A. Electrical Properties of Photochromic Organic Systems. *High Energy Chem.* **2016**, *50*, 371–388.
- (26) Klajn, R. Spiropyran-based Dynamic Materials. Chem. Soc. Rev. 2014, 43, 148–184.
- (27) Irie, M.; Fukaminato, T.; Matsuda, K.; Kobatake, S. Photochromism of Diarylethene Molecules and Crystals: Memories, Switches, and Actuators. *Chem. Rev.* **2014**, *114*, 12174–12277.
- (28) Buback, J.; Nuernberger, P.; Kullmann, M.; Langhojer, F.; Schmidt, R.; Würthner, F.; Brixner, T. Ring-Closure and Isomerization Capabilities of Spiropyran-Derived Merocyanine Isomers. *J. Phys. Chem. A* **2011**, *115*, 3924–3935.
- (29) Dolgopolova, E. A.; Rice, A. M.; Martin, C. R.; Shustova, N. B. Photochemistry and Photophysics of MOFs: Steps Towards MOFbased Sensing Enhancements. *Chem. Soc. Rev.* **2018**, *47*, 4710–4728.
- (30) Kim, D.; Zhang, Z.; Xu, K. Spectrally Resolved Super-Resolution Microscopy Unveils Multipath Reaction Pathways of Single Spiropyran Molecules. *J. Am. Chem. Soc.* **2017**, *139*, 9447–9450.
- (31) Sanchez-Lozano, M.; Estévez, C. M.; Hermida-Ramón, J.; Serrano-Andres, L. Ultrafast Ring-Opening/Closing and Deactivation Channels for a Model Spiropyran—Merocyanine System. *J. Phys. Chem. A* **2011**, *115*, 9128—9138.
- (32) Budyka, M. F. Diarylethylene Photoisomerization and Photocyclization Mechanisms. *Russ. Chem. Rev.* **2012**, *81*, 477–493.
- (33) Mazzucato, U.; Spalletti, A.; Bartocci, G.; Galiazzo, G. Evidence of Adiabatic Channels in the Singlet Photoisomerization of *cis*-1,2-diarylethenes: a Fluorimetric Study. *Coord. Chem. Rev.* **1993**, *125*, 251–260
- (34) Matsuda, K.; Irie, M. J. Diarylethene as a Photoswitching Unit. *J. Photochem. Photobiol.*, C **2004**, *5*, 169–182.
- (35) Nakamura, S.; Yokojima, S.; Uchida, K.; Tsujioka, T. J. Photochromism of Diarylethene: Effect of Polymer Environment and Effects on Surfaces. *J. Photochem. Photobiol., C* **2011**, *12*, 138–150.
- (36) Irie, M. Photochromism of Diarylethene Molecules and Crystals. *Proc. Jpn. Acad., Ser. B* **2010**, *86*, 472–483.
- (37) Pu, S.-Z.; Sun, Q.; Fan, C.-B.; Wang, R.-J.; Liu, G. Recent Advances in Diarylethene-Based Multi-Responsive Molecular Switches. *J. Mater. Chem. C* **2016**, *4*, 3075–3093.
- (38) Fukaminato, T.; Tanaka, M.; Kuroki, L.; Irie, M. Invisible photochromism of diarylethene derivatives. *Chem. Commun.* **2008**, *0*, 3924–3926.
- (39) Williams, D. E.; Martin, C. R.; Dolgopolova, E. A.; Swifton, A.; Godfrey, D. C.; Ejegbavwo, O. A.; Pellechia, P. J.; Smith, M. D.; Shustova, N. B. Flipping the Switch: Fast Photoisomerization in a Confined Environment. *J. Am. Chem. Soc.* **2018**, *140*, 7611–7622.
- (40) López, R.; Gómez, R. Band-Gap Energy Estimation from Diffuse Reflectance Measurements on Sol-Gel and Commercial TiO<sub>2</sub>A comparative study. *J. Sol-Gel Sci. Technol.* **2012**, *61*, 1–7.
- (41) Wudl, F.; Bryce, M. R. Apparatus for Two-Probe Conductivity Measurements on Compressed Powders. *J. Chem. Educ.* **1990**, *67*, 717.
- (42) Dolgopolova, E. A.; Williams, D. E.; Greytak, A. B.; Rice, A. M.; Smith, M. D.; Krause, J. A.; Shustova, N. B. A Bio-inspired Approach

- for Chromophore Communication: Ligand-to-Ligand and Host-to-Guest Energy Transfer in Hybrid Crystalline Scaffolds. *Angew. Chem., Int. Ed.* **2015**, *54*, 13639–13643.
- (43) Liu, J.; Wang, Y.; Benin, A. I.; Jakubczak, P.; Willis, R. R.; LeVan, M. D. CO<sub>2</sub>/H<sub>2</sub>O Adsorption Equilibrium and Rates on Metal-Organic Frameworks: HKUST-1 and Ni/DOBDC. *Langmuir* **2010**, 26, 14301–14307.
- (44) Tam, E. S.; Parks, J. J.; Shum, W. W.; Zhong, Y.-W.; Santiago-Berríos, M. B.; Zheng, X.; Yang, W.; Chan, G. K.-L.; Abruña, H. D.; Ralph, D. C. Single-Molecule Conductance of Pyridine-Terminated Dithienylethene Switch Molecules. *ACS Nano* **2011**, *5*, 5115–5123.
- (45) Williams, D. E.; Rietman, J. A.; Maier, J. M.; Tan, R.; Greytak, A. B.; Smith, M. D.; Krause, J. A.; Shustova, N. B. Energy Transfer on Demand: Photoswitch-Directed Behavior of Metal-Porphyrin Frameworks. J. Am. Chem. Soc. 2014, 136, 11886–11889.
- (46) Zheng, Y.; Sato, H.; Wu, P.; Jeon, H. J.; Matsuda, R.; Kitagawa, S. Flexible Interlocked Porous Frameworks Allow Quantitative Photoisomerization in a Crystalline Solid. *Nat. Commun.* **2017**, *8*, 100.
- (47) Nikolayenko, V. I.; Herbert, S. A.; Barbour, L. J. Reversible Structural Switching of a Metal-Organic Framework by Photoirradiation. *Chem. Commun.* **2017**, *53*, 11142–11145.
- (48) Luo, F.; Fan, C. B.; Luo, M. B.; Wu, X. L.; Zhu, Y.; Pu, S. Z.; Xu, W. Y.; Guo, G. C. Photoswitching CO<sub>2</sub> Capture and Release in a Photochromic Diarylethene Metal—Organic Framework. *Angew. Chem., Int. Ed.* **2014**, *53*, 9298–9301.
- (49) Mendoza, S. M.; Lubomska, M.; Walko, M.; Feringa, B. L.; Rudolf, P. Characterization by X-ray Photoemission Spectroscopy of the Open and Closed Forms of a Dithienylethene Switch in Thin Films. *J. Phys. Chem. C* **2007**, *111*, 16533–16537.
- (50) Cressie, N. A. C.; Whitford, H. J. How to Use the Two Sample *t*-Test. *Biom. J.* **1986**, 28, 131–148.
- (51) Yuan, S.; Lu, W.; Chen, Y.-P.; Zhang, Q.; Liu, T.-F.; Feng, D.; Wang, X.; Qin, J.; Zhou, H.-C. Sequential Linker Installation: Precise Placement of Functional Groups in Multivariate Metal-Organic Frameworks. J. Am. Chem. Soc. 2015, 137, 3177–3180.
- (52) Dulić, D.; van der Molen, S. J.; Kudernac, T.; Jonkman, H. T.; de Jong, J. J. D.; Bowden, T. N.; van Esch, J.; Feringa, B. L.; van Wees, B. J. One-Way Optoelectronic Switching of Photochromic Molecules on Gold. *Phys. Rev. Lett.* **2003**, *91*, 207402.
- (53) Farha, O. K.; Malliakas, C. D.; Kanatzidis, M. G.; Hupp, J. T. Control over Catenation in Metal—Organic Frameworks via Rational Design of the Organic Building Block. *J. Am. Chem. Soc.* **2010**, *132*, 950–952.
- (54) Chen, D.; Xing, H.; Su, Z.; Wang, C. Electrical Conductivity and Electroluminescence of a New Anthracene-based Metal-Organic Framework with  $\pi$ -conjugated Zigzag Chains. *Chem. Commun.* **2016**, 52, 2019–2022.
- (55) Wiebeler, C.; Bader, C. A.; Meier, C.; Schumacher, S. Optical Spectrum, Perceived Color, Refractive Index, and Non-Adiabatic Dynamics of the Photochromic Diarylethene CMTE. *Phys. Chem. Chem. Phys.* **2014**, *16*, 14531–14538.
- (56) Wiebeler, C.; Schumacher, S. Quantum Yields and Reaction Times of Photochromic Diarylethenes: Nonadiabatic Ab Initio Molecular Dynamics for Normal- and Inverse-Type. *J. Phys. Chem.* A **2014**, *118*, 7816–7823.
- (57) Kim, M.; Yun, J.-H.; Cho, M. Light Penetration-Coupled Photoisomerization Modeling for Photodeformation of Diarylethene Single Crystal: Upscaling Isomerization to Macroscopic Deformation. *Sci. Rep.* **2017**, *7*, 967.
- (58) Grimme, S.; Antony, J.; Ehrlich, S.; Krieg, H. A Consistent and Accurate *ab initio* Parametrization of Density Functional Dispersion Correction (DFT-D) for the 94 Elements H-Pu. *J. Chem. Phys.* **2010**, 132, 154104.
- (59) Shao, Y.; Gan, Z.; Epifanovsky, E.; Gilbert, A. T. B.; Wormit, M.; Kussmann, J.; Lange, A. W.; Behn, A.; Deng, J.; Feng, X.; Ghosh, D.; Goldey, M.; Horn, P. R.; Jacobson, L. D.; Kaliman, I.; Khaliullin, R. Z.; Kuś, T.; Landau, A.; Liu, J.; Proynov, E. I.; Rhee, Y. M.; Richard, R. M.; Rohrdanz, M. A.; Steele, R. P.; Sundstrom, E. J.; Woodcock, H. L.; Zimmerman, P. M.; Zuev, D.; Albrecht, B.; Alguire,

- E.; Austin, B.; Beran, G. J. O.; Bernard, Y. A.; Berquist, E.; Brandhorst, K.; Bravaya, K. B.; Brown, S. T.; Casanova, D.; Chang, C.-M.; Chen, Y.; Chien, S. H.; Closser, K. D.; Crittenden, D. L.; Diedenhofen, M.; DiStasio, R. A.; Do, H.; Dutoi, A. D.; Edgar, R. G.; Fatehi, S.; Fusti-Molnar, L.; Ghysels, A.; Golubeva-Zadorozhnava, A.; Gomes, J.; Hanson-Heine, M. W. D.; Harbach, P. H. P.; Hauser, A. W.; Hohenstein, E. G.; Holden, Z. C.; Jagau, T.-C.; Ji, H.; Kaduk, B.; Khistyaev, K.; Kim, J.; Kim, J.; King, R. A.; Klunzinger, P.; Kosenkov, D.; Kowalczyk, T.; Krauter, C. M.; Lao, K. U.; Laurent, A. D.; Lawler, K. V.; Levchenko, S. V.; Lin, C. Y.; Liu, F.; Livshits, E.; Lochan, R. C.; Luenser, A.; Manohar, P.; Manzer, S. F.; Mao, S.-P.; Mardirossian, N.; Marenich, A. V.; Maurer, S. A.; Mayhall, N. J.; Neuscamman, E.; Oana, C. M.; Olivares-Amaya, R.; O'Neill, D. P.; Parkhill, J. A.; Perrine, T. M.; Peverati, R.; Prociuk, A.; Rehn, D. R.; Rosta, E.; Russ, N. J.; Sharada, S. M.; Sharma, S.; Small, D. W.; Sodt, A.; Stein, T.; Stück, D.; Su, Y.-C.; Thom, A. J. W.; Tsuchimochi, T.; Vanovschi, V.; Vogt, L.; Vydrov, O.; Wang, T.; Watson, M. A.; Wenzel, J.; White, A.; Williams, C. F.; Yang, J.; Yeganeh, S.; Yost, S. R.; You, Z.-Q.; Zhang, I. Y.; Zhang, X.; Zhao, Y.; Brooks, B. R.; Chan, G. K. L.; Chipman, D. M.; Cramer, C. J.; Goddard, W. A.; Gordon, M. S.; Hehre, W. J.; Klamt, A.; Schaefer, H. F.; Schmidt, M. W.; Sherrill, C. D.; Truhlar, D. G.; Warshel, A.; Xu, X.; Aspuru-Guzik, A.; Baer, R.; Bell, A. T.; Besley, N. A.; Chai, J.-D.; Dreuw, A.; Dunietz, B. D.; Furlani, T. R.; Gwaltney, S. R.; Hsu, C.-P.; Jung, Y.; Kong, J.; Lambrecht, D. S.; Liang, W.; Ochsenfeld, C.; Rassolov, V. A.; Slipchenko, L. V.; Subotnik, J. E.; Van Voorhis, T.; Herbert, J. M.; Krylov, A. I.; Gill, P. M. W.; Head-Gordon, M. Advances in Molecular Quantum Chemistry Contained in the Q-Chem 4 Program Package. Mol. Phys. 2015, 113, 184-215.
- (60) Zhuang, M.; Ernzerhof, M. Reversibility and Transport Properties of Dithienylethene Photoswitches. J. Chem. Phys. 2009, 130, 114704.
- (61) Huang, J.; Li, Q.; Ren, H.; Su, H.; Shi, Q. W.; Yang, J. Switching Mechanism of Photochromic Diarylethene Derivatives Molecular Junctions. *J. Chem. Phys.* **2007**, *127*, 094705.
- (62) Kondo, M.; Tada, T.; Yoshizawa, K. A Theoretical Measurement of the Quantum Transport Through an Optical Molecular Switch. *Chem. Phys. Lett.* **2005**, 412, 55–59.
- (63) Frisch, J.; Herder, M.; Herrmann, P.; Heimel, G.; Hecht, S.; Koch, N. Photoinduced Reversible Changes in the Electronic Structure of Photochromic Diarylethene Films. *Appl. Phys. A: Mater. Sci. Process.* **2013**, *113*, 1–4.
- (64) Wang, Q.; Frisch, J.; Herder, M.; Hecht, S.; Koch, N.; Risch, J.; Martin, H.; Hecht, S.; Koch, A. Electronic Properties of Optically Switchable Photochromic Diarylethene Molecules at the Interface with Organic Semiconductors. *ChemPhysChem* **2017**, *18*, 722–727.